JOURNAL OF CATALYSIS 156, 106–119 (1995)

The Oxidative Coupling of Methane over MgO-Based Catalysts: A Steady-State Isotope Transient Kinetic Analysis

R. H. Nibbelke, J. Scheerová, M. H. J. M. de Croon, and G. B. Marin[1]

Schuit Institute of Catalysis, Eindhoven University of Technology, P.O. Box 513, 5600 MB Eindhoven, The Netherlands

Received August 15, 1994; revised March 21, 1995

To study the heterogeneous steps of the oxidative coupling of methane to ethane and ethene over MgO, Li/MgO and Sn/Li/MgO, oxygen and carbon dioxide isotope step experiments were carried out in the absence of reaction, and oxygen and methane isotope step experiments were carried out in a tubular reactor at 1023 K, atmospheric pressure, an inlet molar ratio of CH_4/O_2 equal to 4, a methane conversion of 24%, and an oxygen conversion of 85%. The steady-state axial total concentration profiles of the reactants, intermediates, and products have a significant influence on the shapes of the transient isotope responses under these conditions. Oxygen interacts strongly with all catalysts used by dissociative reversible adsorption, except for lined-out Li/MgO. Both surface and bulk lattice oxygen participate in the reaction. The promotion with lithium and even more with tin increases the mobility of oxygen in the bulk of the catalyst and the amount of exchangeable oxygen per unit BET surface area. Carbon in methane can either react to C_2 products, without any significant interaction with the catalyst, or show a weak reversible interaction with the catalyst, which does not lead to C_2 products. In the absence of reaction, carbon dioxide interacts with the catalyst only in the presence of lithium. Under reaction conditions, the experiments can be described satisfactorily by postulating a methoxy species as the only carbon-containing intermediate on the catalyst leading to carbon dioxide.

INTRODUCTION

The oxidative coupling of methane aims at the production of ethane, ethene, and higher hydrocarbons, abbreviated as C_{2+} products, from methane and oxygen. The undesired reaction is the oxidation of hydrocarbons to carbon monoxide and carbon dioxide. Although coupling also occurs without a catalyst (1–3) the process is usually carried out in the presence of a catalyst to obtain sufficient activity and selectivity to the desired products. In order to optimize the catalyst performance, insight into the heterogeneous and homogeneous reaction steps constituting the mechanism is required. The aim of the investigation presented here is to study the heterogeneous steps of the oxidative coupling of methane over MgO-based catalysts using steady-state isotope transient kinetic analysis (SSITKA). This technique, advocated by Happel (4) and Biloen *et al.* (5) can yield information about the heterogeneous steps in a reaction mechanism under steady-state conditions without interference of the homogeneous steps. Experimentally the decay or development of isotopically labelled products and reactants is monitored by a mass spectrometer after switching between reactant isotopes in the feed stream, without changing the operating conditions (6). If kinetic isotope effects can be neglected the steady state will not be disturbed. The shapes of the transient responses of labelled and unlabelled reactants and products give information about the reaction pathways of the labelled atoms. The areas under the transient curves give information about the amounts of species bound to the catalyst. The SSITKA technique has been applied recently to study the oxidative coupling of methane (7–16). The main conclusions drawn for MgO and Li/MgO are (8, 9, 11, 12) dissociative adsorption of oxygen, the participation of both surface and bulk lattice oxygen in the reaction, and only a small interaction of carbon with the catalyst in both methane and ethane. A strong interaction of carbon atoms with the catalyst leading to carbon dioxide was observed, indicating readsorption of carbon dioxide or a surface oxidation pathway to carbon dioxide. In this study oxygen, carbon dioxide, and methane isotope step experiments over MgO, Li/MgO, and Sn/Li/MgO are presented. Special attention is paid to the effects of the promotion with lithium and tin, the interaction of carbon dioxide with the catalyst and the reaction pathway to carbon dioxide.

The experimental results are not only discussed in qualitative terms. Isotope transients can be described quantitatively in terms of surface concentrations and rates of elementary reaction steps. This is especially helpful in the selection of a sound kinetic model, because of the severe requirements that the transient responses impose on such a model. In an ideal isothermal plug flow reactor the continuity equations for the isotopically labelled components

[1] To whom correspondence should be addressed.

0021-9517/95 $12.00

TABLE 1

BET Surface Areas with Their 66% Confidence Intervals and Elemental Composition of Fresh and Lined-Out Li/MgO and Sn/Li/MgO

	Li/MgO		Sn/Li/MgO	
	Fresh	Lined-out	Fresh	Lined-out
BET surface area (m^2_{CAT} kg^{-1}_{CAT})	600 ± 300	850 ± 300	2000 ± 300	2740 ± 300
Li/wt.%	3.7	0.6	4.8	3.5
Sn/wt.%	—	—	3.0	2.6
Mg/wt.%	33	59	39.8	40.0

in the gas phase and on the catalyst are partial differential equations (17). Moreover, under reaction conditions it may be necessary to take the steady-state total concentration profiles along the reactor axis into account. These steady-state axial total concentration profiles can be described with a set of ordinary differential equations for the gas-phase components and a set of algebraic equations for the species present on the catalyst. Usually the set of model equations can only be solved numerically. Kinetic parameters, such as reaction rate coefficients, surface concentrations, and diffusion coefficients, can be estimated by regression of the experimental data using nonlinear regression analysis. The most reliable model is developed if different kinds of isotope step experiments are regressed simultaneously, i.e., described with a single set of kinetic parameters. The present work follows the above approach.

EXPERIMENTAL

Catalysts

The catalysts used in this investigation are MgO, lithium-promoted MgO, and tin/lithium-promoted MgO. The preparation of these catalysts is described elsewhere (18). For the promoted catalysts, a line-out procedure was applied to reach a stable level of conversions and selectivities over a sufficiently long period of time (19). It consisted of maintaining the following conditions for 12 h: atmospheric pressure; an inlet molar ratio CH_4/O_2 equal to 4; a space time, defined as the catalyst mass divided by the total molar flow rate, of 1.7 kg_{CAT} s mol^{-1}; a dilution ratio of 10 kg α-Al_2O_3 per kilogram of catalyst; and a temperature of 1123 K for Li/MgO and 1023 K for Sn/Li/MgO. For the isotope step experiments both the fresh and the lined-out catalysts were used. The BET surface areas and the elemental composition of Li/MgO and Sn/Li/MgO are presented in Table 1. The BET surface area of pure MgO amounted to 28900 m^2_{CAT} kg^{-1}_{CAT}.

Equipment

Feed section. Helium (0.99995) was used as a diluent and argon (0.999990) was used as a tracer to give indications of the deviation from plug flow. Oxygen (0.995), methane (0.995), and carbon dioxide (0.995) were used as feed gases. $^{18}O_2$(0.995), $^{13}CO_2$(0.99), and $^{13}CH_4$(0.99) were used in the isotope step experiments. Two gas mixtures can be created which are identical except for the fact that in one of these mixtures a component is replaced by an isotope and that in the gas mixture with the unlabelled component a trace amount of argon is present. A four-way valve upstream from the reactor makes it possible to switch between the two gas mixtures realising an isotope step from the unlabelled to the labelled component.

Reactor section. A quartz fixed-bed microreactor with an internal diameter of 9 mm and a length of 18 cm was used in this study. Typically 0.25 g of catalyst was placed on a porous quartz filter. The dead volume in the precatalytic space was filled with quartz particles to minimize back-mixing effects. The postcatalytic volume was minimized by a narrowing of the reactor tube. The reactor was heated by an electrical oven and the reaction temperature was measured with a thermocouple placed in a well in the catalyst bed. The response of the inert argon tracer after a step He → He/Ar at a total molar flow rate of 3.5×10^{-5} mol s^{-1} can be described satisfactorily with the empirical function

$$f(t) = \frac{1 - e^{-0.77t}}{1 + e^{-0.77t}}, \qquad [1]$$

where t is the time after switching (s). Equation [1] describes the fraction of argon observed at the outlet of the reactor as a function of time. Because of the small height of the catalyst bed, approximately 3 mm, as compared to the height of the bed of inert quartz particles upstream from the catalyst bed, approximately 10 cm, the function presented by Eq. [1] is a good approximation of the signal at the inlet of the catalyst bed.

Analysis section. A quadrupole mass spectrometer (VG Quadrupoles, Sensor Lab 200D) coupled with a computerized data acquisition system was used to monitor the transient responses of the different isotopes. In this work the mass spectrometer performed typically five measurements per second. The mass spectrometer data were corrected for background values and normalized to isotope fractions such that the sum of the isotope fractions equals one.

Under reaction conditions the reactor effluent was analyzed by a Carlo Erba gas chromatograph (VEGA SERIES 2). In a column packed with Porapack Q, methane and carbon dioxide were separated and detected by a thermal

conductivity detector (TCD). In a column packed with molsieve 5A, methane and oxygen were separated and detected by a TCD. In a column packed with Porasil C, methane, ethane, ethene, and propane were separated and detected by a flame ionization detector (FID). The methane conversion and the selectivities were calculated with the normalization method, i.e., a 100% carbon balance was assumed. As no internal standard was added, this assumption could not be verified. The oxygen conversion could not be calculated using the normalization method as not all oxygen-containing components, i.e., water, were measured. Therefore the oxygen outlet flow rate was calculated from the methane outlet flow rate using the gas chromatograph calibration factors and the peak areas of both components.

Procedure

Before starting the isotope step experiments in the absence of reaction, the catalyst was pretreated overnight with an oxygen flow rate of 6.8×10^{-6} mol s^{-1} at 1123 K to remove adsorbed water and carbon dioxide. Next the temperature was decreased to the experimental temperature and the oxygen flow was replaced by a helium flow. All experiments presented in this study were carried out at atmospheric pressure, a temperature of 1023 K, with an initial total molar flow rate of 3.5×10^{-5} mol s^{-1}, an argon flow rate of 3.5×10^{-6} mol s^{-1} and 0.25 g of catalyst. In the absence of reaction the flow was diluted with 96–98% helium. Before starting an isotope step experiment under reaction conditions, the catalyst was heated under a helium flow until the desired experimental temperature was reached. Under reaction conditions, experiments were only carried out over the lined-out Li/Sn/MgO catalyst. These experiments were carried out at an initial molar ratio CH_4/O_2 equal to 4 and with 80% helium dilution. Under these conditions both C_{2+} products and carbon dioxide were observed. The methane and oxygen conversion and the selectivities towards the observed products with respect to methane were as follows: $X_{CH_4} = 24\%$, $X_{O_2} = 85\%$, $S_{C_2H_6} = 31\%$, $S_{C_2H_4} = 23\%$, $S_{C_3H_8} = 2\%$, and $S_{CO_2} = 44\%$.

Before the isotope switch was performed, the reactor was fed with the mixture containing the unlabelled component until steady-state conditions were achieved, typically within 60 min. After switching to the mixture with the isotopically labelled component, the transient isotopic responses were monitored for a period of typically 5 min.

METHODS OF DATA EVALUATION

Reactor Modelling

The reactor can be considered to be isothermal and isobaric. Hence, the reactor model is reduced to a set of continuity equations for the species involved. If kinetic isotope effects can be neglected, the sum of the concentrations of all isotopes of a component is constant at a given position in the reactor throughout the experiment and only the continuity equations for the labelled components need to be considered. The fixed-bed reactor is assumed to be of the plug flow type, because a value of 16 was obtained for the Péclet number based on the total tube length from the response of an inert component to a step. The total molar flow rate can be assumed to be constant through the bed, because of the high dilution of the flow with inert gas. Intra- and interparticle gradients are assumed to have no significant influence on the transient isotope responses. With these assumptions the continuity equations for labelled gas-phase component i' and labelled species j' on the catalyst are as follows:

$$\frac{\partial C_{i'}(x,t)}{\partial t} + \frac{1}{\tau}\frac{\partial C_{i'}(x,t)}{\partial x} = \frac{\rho_B}{\varepsilon_B} R_{i'}(x,t) \qquad [2]$$

$$\frac{\partial L_{j'}(x,t)}{\partial t} = R_{j'}(x,t). \qquad [3]$$

For an isotope step from gas-phase component k to k', the initial and boundary conditions are

Initial conditions:

$$t = 0 \quad \forall x \qquad C_{i'} = L_{j'} = 0 \qquad [4a]$$

Boundary conditions:

$$t > 0 \quad x = 0 \quad C_{k'} = \text{input function } (t) \qquad [4b]$$

$$t > 0 \quad x = 0 \quad C_{i'} = 0 \text{ for } i' \neq k', \qquad [4c]$$

where $C_{i'}$ is the concentration of labelled gas-phase component i' (mol m_{gas}^{-3}); $L_{j'}$ is the concentration of labelled surface species j' (mol kg_{CAT}^{-1}); t is the time (s); τ is the residence time in the reactor (s); x is the dimensionless axial reactor position, defined as the cumulative catalyst mass at the corresponding position divided by the total catalyst mass W_{CAT} (kg_{CAT}); ρ_B is the bed density (kg_{CAT} m_{bed}^{-3}); ε_B is the bed porosity (m_{gas}^3 m_{bed}^{-3}); $R_{i'}$ is the net production rate of labelled gas-phase component i' (mol kg_{CAT}^{-1} s^{-1}); and $R_{j'}$ is the net production rate of labelled surface species j' (mol kg_{CAT}^{-1} s^{-1}). The residence time τ in the reactor is calculated as $\tau = \varepsilon_B W_{CAT}/\rho_B F_{TOT} V_{mol}$ where F_{TOT} is the total molar flow rate (mol s^{-1}) and V_{mol} is the molar volume (m_{gas}^3 mol^{-1}) at the reactor conditions. In this study the input function is given by Eq [1]. Generally the production rates $R_{i'}$ and $R_{j'}$ are linear combinations of the reaction rates of the elementary steps in which labelled gas-phase component i' or labelled surface species j' is involved, and hence are determined by the corresponding kinetic parameters.

The set of partial differential Equations [2]–[4] is integrated using an adaptive moving grid method. This method is especially suited for solving initial boundary problems for sets of one-space dimensional partial differential equations the solutions of which exhibit rapid variations in space and time (20). In the present study, this procedure was implemented in a standard integration routine from the Numerical Algorithm Group (21) for integrating stiff systems of implicit ordinary differential equations coupled with algebraic equations (routine D02NHF). An integration takes typically 15 min of CPU time on a Silicon Graphics Power Challenge.

Under reaction conditions it may be necessary to take the steady-state axial total concentration profiles into account. This is required if the latter have a significant influence on the reaction rates, i.e., if the reactor is operated in an integral way. At the steady state the continuity equation for the sum of an unlabelled and a labelled gas-phase component can be written as

$$\frac{dC_{(i+i')}(x)}{dx} = \frac{\rho_B \tau}{\varepsilon_B} R_{(i+i')}(x), \qquad [5]$$

where $C_{(i+i')}$ is the steady-state total concentration of the unlabelled and labelled gas-phase component (mol m_{gas}^{-3}), $R_{(i+i')}$ is the steady-state total net production rate of the unlabelled and labelled gas-phase component (mol $kg_{CAT}^{-1}\ s^{-1}$), and $C_{(i+i')} = C^0_{(i+i')}$ at $x = 0$ as the initial condition.

At the steady state, the continuity equation for the sum of an unlabelled and labelled species on the catalyst reduces to the algebraic equation

$$R_{(j+j')}(x) = 0, \qquad [6]$$

where $R_{(j+j')}$ is the steady-state total net production rate of unlabelled and labelled species on the catalyst (mol $kg_{CAT}^{-1}\ s^{-1}$).

Integrating the continuity equations for the gas-phase components, Eq. [5], and simultaneously solving the algebraic equations for the species on the catalyst, Eq. [6], leads to the steady-state axial total concentration profiles for both the gas-phase components and the species on the catalyst. The ordinary differential equations, Eq. [5], are integrated using a Runge–Kutta–Merson method. The algebraic equations, Eq. [6], are solved with a modified Powell hybrid method. Both methods were taken from the Numerical Algorithm Group (21) (routines D02BBF and C05NBF, respectively.)

Regression Analysis

The estimation of the kinetic parameters was performed by minimization of the objective function

$$S(\mathbf{b}) = \sum_{q=1}^{v}\sum_{r=1}^{v} \sigma^{qr} \sum_{i=1}^{n} [y_{i,q} - f_q(\mathbf{x}_i, b)][y_{i,r} - f_r(\mathbf{x}_i, \mathbf{b})] \rightarrow \text{minimum}, \qquad [7]$$

where S is the objective function; σ^{qr} is an element of the inverse error covariance matrix; $y_{i,q}$ is the qth experimental response, either an isotope fraction or a concentration, in the ith experiment; $y_{i,r}$ is the rth experimental response in the ith experiment; $f_q(\mathbf{x}_i, \mathbf{b})$ is the response value calculated with the reactor model for response q of experiment i; $f_r(\mathbf{x}_i, \mathbf{b})$ is the response value calculated with the reactor model for response r of experiment i; $\mathbf{x}_i$ is the vector of set variables for experiment i; $\mathbf{b}$ is the parameter vector; v is the number of responses; and n is the number of experiments. The objective function is based upon the assumption that the experimental errors are normally distributed with a zero mean. The minimization of the objective function was achieved with a multiresponse Marquardt algorithm (22, 23). The elements σ^{qr} of the inverse error covariance matrix are estimated by the regression routine following a first regression with a unit error covariance matrix. For the experiments in the absence of reaction the isotope fractions of the labelled components were regressed. For the experiments under reaction conditions the concentrations of the labelled components, i.e., the isotope fraction multiplied by the steady-state outlet concentration, were regressed because this allowed for the estimation of more parameters than if isotope fractions were regressed. Indeed, regression of the concentrations takes into account observed conversions and selectivities.

The parameter estimates were tested for statistical significance on the basis of their individual t values. The statistical significance of the global regression was expressed by means of the so-called F test, which is based on the comparison of the sum of squares of the calculated response values and the residual sum of squares. A high F value corresponds to a high significance of the global regression. Discrimination among rival models was based on this statistical testing, whenever it was not possible by direct observation or by physicochemical laws. A detailed description of the regression analysis procedure is given by Froment and Hosten (23).

EXPERIMENTAL RESULTS

Oxygen Isotope Steps in the Absence of Reaction

Oxygen isotope steps, $^{16}O_2 \rightarrow {}^{18}O_2$, were carried out in the absence of reaction to study the interaction of oxygen with the catalyst and to determine the effects of promotion with lithium and tin on the amount of exchangeable oxygen and the mobility of lattice oxygen in the bulk of the catalyst. The catalysts used for the experiments were MgO, fresh and lined-out Li/MgO, and fresh and lined-out Sn/Li/

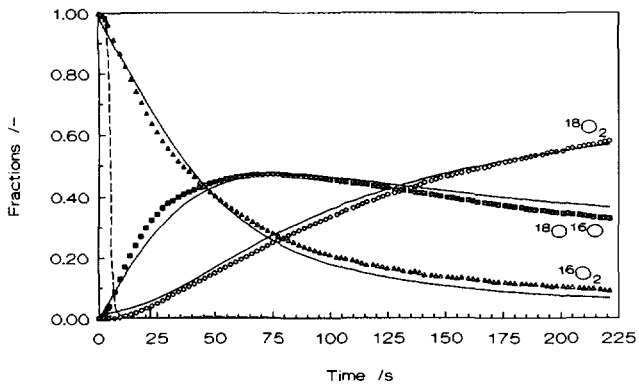

FIG. 1. Oxygen responses after step $^{16}O_2 \rightarrow {}^{18}O_2$ (no reaction) over fresh Li/Sn/MgO; T = 1023 K; 1.8% O_2. Dashed line, argon; Δ, $^{16}O_2$; ■, $^{18}O^{16}O$; ○, $^{18}O_2$; full lines, calculated with the set of parameter estimates given in Table 3 by integration of Eqs. [2] and [3] with the corresponding net production rates [8], [9], and [12].

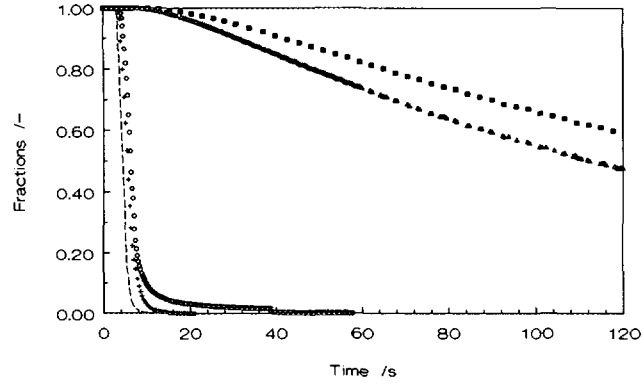

FIG. 2. $^{12}CO_2$ responses after step $^{12}CO_2 \rightarrow {}^{13}CO_2$ (no reaction) over various catalysts; T = 1023 K. Dashed line, argon; +, MgO (3 mol% CO_2); ○, lined-out Li/MgO (2 mol% CO_2); Δ, fresh Li/MgO (3 mol% CO_2); ■, fresh Li/Sn/MgO (3 mol% CO_2).

MgO. No significant exchange was observed in the absence of catalyst. For all catalysts, except for the lined-out Li/MgO catalyst, similar transient isotope responses were obtained. As an example, the transient isotope responses and the argon tracer of the experiment over fresh Sn/Li/MgO are shown in Fig. 1. The $^{16}O_2$ response is slow as compared to the inert response, indicating a strong interaction of oxygen with the catalyst. The $^{16}O^{18}O$ response decreases slowly after reaching a maximum and tends to a relatively stable level. The formation of $^{16}O^{18}O$ indicates the dissociative adsorption of oxygen. The relatively stable level of the $^{16}O^{18}O$ signal indicates that an extra oxygen source is available for exchange besides oxygen in the gas phase. This extra oxygen source must be lattice oxygen in the bulk of the oxide catalyst. No significant exchange was observed with lined-out Li/MgO, indicating a very weak interaction of oxygen with this catalyst or none at all.

Carbon Dioxide Isotope Steps in the Absence of Reaction

Carbon dioxide isotope steps, $^{12}CO_2 \rightarrow {}^{13}CO_2$, were carried out in the absence of reaction to study the interaction of carbon dioxide with the catalyst and the effects of promotion with lithium and tin on this interaction. The catalysts used for the experiments were MgO, fresh and lined-out Li/MgO, and fresh Sn/Li/MgO. The $^{12}CO_2$ responses of the experiments over the various catalysts are shown in Fig. 2. The $^{13}CO_2$ responses are not shown but can be calculated easily, remembering that by definition the sum of the $^{12}CO_2$ and the $^{13}CO_2$ fractions equals one. For MgO and lined-out Li/MgO the $^{12}CO_2$ response only slightly trails the inert response indicating only a small interaction of carbon dioxide with these catalysts. The $^{12}CO_2$ responses over fresh Li/MgO and Sn/Li/MgO are very slow as compared to the inert response indicating a strong interaction of carbon dioxide with these catalysts.

Isotope Steps in the Presence of Reaction

Oxygen isotope steps. The oxygen isotope step experiment, $^{16}O_2/CH_4 \rightarrow {}^{18}O_2/CH_4$, was carried out under reaction conditions to study the reaction pathways to the oxygen-containing products and the interaction of oxygen with lined-out Sn/Li/MgO under reaction conditions. The oxygen and carbon dioxide isotope responses are shown in Figs. 3 and 4. In contrast to the oxygen isotope responses of the experiment over lined-out Sn/Li/MgO in the absence of reaction, not shown but similar to the responses shown in Fig. 1, the oxygen responses under reaction conditions initially display a rapid relaxation, not significantly different from the inert response. This could be the result of the presence of water, carbon dioxide, or a carbonate phase on the catalyst under reaction conditions, diminish-

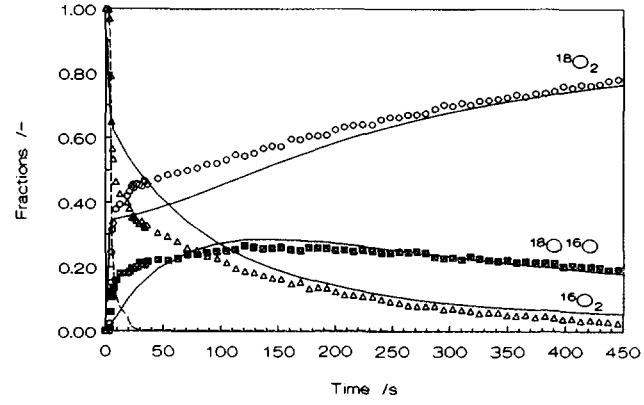

FIG. 3. Oxygen responses after step $^{16}O_2/CH_4 \rightarrow {}^{18}O_2/CH_4$ over lined-out Li/Sn/MgO; T = 1023 K; $(CH_4/O_2)|_0 = 4$; X_{CH_4} = 24%; X_{O_2} = 85%; $S_{C_2H_6}$ = 31%; $S_{C_2H_4}$ = 23%; $S_{C_3H_8}$ = 2%; S_{CO_2} = 44%. Dashed line, argon; Δ, $^{16}O_2$; ■, $^{16}O^{18}O$; ○, $^{18}O_2$; full lines, calculated with the set of parameters given in Table 4 by integration of Eqs. [2] and [3] with the corresponding net production rates [8]–[13].

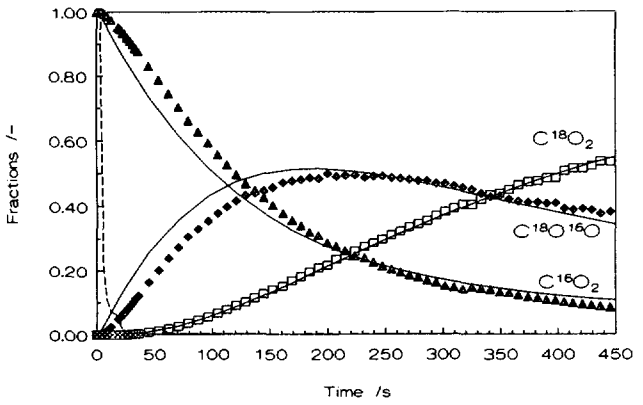

FIG. 4. Carbon dioxide responses after step $^{16}O_2/CH_4 \rightarrow {}^{18}O_2/CH_4$ over lined-out Li/Sn/MgO; T = 1023 K; $(CH_4/O_2)|_0$ = 4; X_{CH_4} = 24%; X_{O_2} = 85%; $S_{C_2H_6}$ = 31%; $S_{C_2H_4}$ = 23%; $S_{C_3H_8}$ = 2%; S_{CO_2} = 44%. Dashed line, argon; ▲, $C^{16}O_2$; ◆, $C^{16}O^{18}O$; □, $C^{18}O_2$; full lines, calculated with the set of parameters given in Table 4 by integration of Eqs. [2] and [3] with the corresponding net production rates [8]–[13].

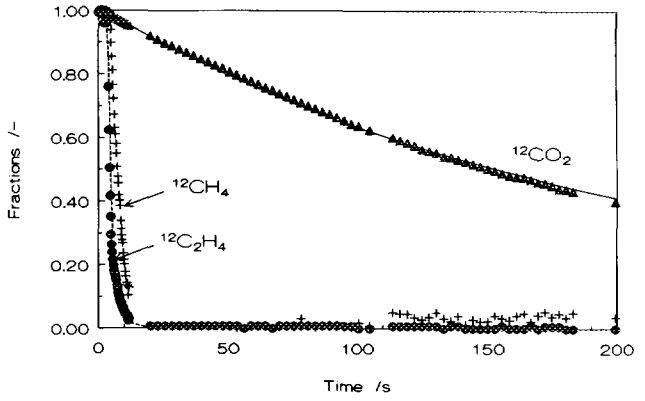

FIG. 6. $^{12}CH_4$, $^{12}C_2H_4$, and $^{12}CO_2$ responses after step $O_2/^{12}CH_4 \rightarrow O_2/^{13}CH_4$ over stabilized Li/Sn/MgO; T = 1023 K; $(CH_4/O_2)|_0$ = 4; X_{CH_4} = 24%; X_{O_2} = 85%; $S_{C_2H_6}$ = 31%; $S_{C_2H_4}$ = 23%; $S_{C_3H_8}$ = 2%; S_{CO_2} = 44%. Dashed line, argon; ●, $^{12}C_2H_4$; +, $^{12}CH_4$; ▲, $^{12}CO_2$; full line, calculated with the set of parameters given in Table 4 by integration of Eqs. [2] and [3] with the corresponding net production rates [14]–[16].

ing the number of exchange sites for oxygen. Alternatively, a fast reaction of oxygen on the catalyst with carbon species could hinder a strong interaction of oxygen with the catalyst. In Fig. 5, the value of the ratio $C^2_{16_O18_O}/C_{18_{O_2}}C_{16_{O_2}}$ versus time is given for the oxygen isotope step experiments over lined-out Sn/Li/MgO both in the absence and in the presence of reaction. The value of the ratio is equal to 4 if the oxygen isotopes are in statistical equilibrium (24–26). In the absence of reaction the value of the factor tends to 4 while in the presence of methane nonstatistical mixing of the oxygen isotopes can be observed. These observations are in agreement with the experiments carried out by Peil *et al.* (8) over Li/MgO. The fact that under reaction conditions the oxygen atoms are not statistically mixed could be rationalised by a limited surface mobility

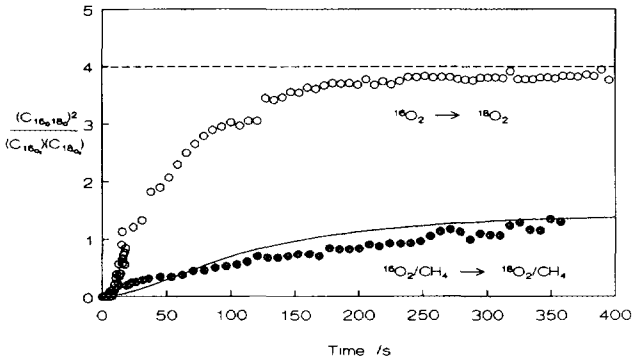

FIG. 5. The ratio $C^2_{16_O18_O}/C_{18_{O_2}}C_{16_{O_2}}$ versus time for the oxygen isotope step experiments over lined-out Li/Sn/MgO in the absence (○) and in the presence (●) of reaction. Full line, calculated by integration of Eqs. [2] and [3] with the corresponding net production rates [8] to [13] and the parameter estimates given in Table 4.

of adsorbed oxygen atoms due to other adsorbed species, but this hypothesis cannot explain the initial rapid relaxation of the oxygen isotope responses under reaction conditions. The differences between the oxygen isotope responses in the absence and in the presence of reaction will be further addressed during the discussion of the modelling results.

The $C^{16}O_2$ response is slow as compared to the inert response, indicating a strong interaction with the catalyst of oxygen atoms leading to carbon dioxide. Similar to the $^{16}O^{18}O$ response, the $C^{16}O^{18}O$ response tends to a relatively stable level after reaching a maximum, indicating the participation of lattice oxygen from the bulk of the catalyst in the formation of carbon dioxide. The oxygen atoms ending up in carbon dioxide remain on the catalyst long enough to provide statistical mixing of the carbon dioxide isotopes. The interaction of these oxygen atoms with the catalyst is caused by the primary formation of CO_2 and/or by readsorption of carbon dioxide as a carbonate phase.

Methane isotopes steps. The methane isotope step experiment, $O_2/^{12}CH_4 \rightarrow O_2/^{13}CH_4$, was carried out under reaction conditions to study the reaction pathways to the carbon-containing products and the interaction of methane with lined-out Sn/Li/MgO. The resulting transient isotope responses of the unlabelled components, $^{12}CH_4$, $^{12}C_2H_4$, and $^{12}CO_2$, are shown in Fig. 6. Monitoring of other components was not possible because of mass resolution limitations.

The $^{12}C_2H_4$ transient relaxes together with the inert response indicating the lack of significant interaction with the catalyst of carbon-containing species leading to ethene. The $^{12}CH_4$ transient only slightly trails the inert response

TABLE 2

Reaction Mechanism Used for Describing the Isotope Step Experiments on Line-Out Sn/Li/MgO

1. $\mathbf{O_2 + 2* \underset{k_{-1}}{\overset{k_1}{\rightleftarrows}} 2O*}$

2. $\mathbf{CH_4 + O* \xrightarrow{k_2} CH_3\cdot + OH*}$

3. $OH* + OH* \rightarrow H_2O + O* + *$

4. $\mathbf{CH_3\cdot + CH_3\cdot \xrightarrow{k_4} C_2H_6}$

5. $\mathbf{C_2H_6 + O* \xrightarrow{k_5} C_2H_5\cdot + OH*}$

6. $C_2H_5\cdot + O* \rightarrow C_2H_4 + OH*$

7. $\mathbf{CH_3\cdot + O* \xrightarrow{k_7} CH_3O*}$

8. $\mathbf{CH_3O* + O* \xrightarrow{k_8} CH_2O* + OH*}$

9. $CH_2O* + 3O* \rightarrow CO_2 + 3OH* + *$

10. $\mathbf{O* \underset{c_0}{\overset{c_0}{\rightleftarrows}} O_{BULK}}$

Note. The kinetically significant reactions are depicted in bold, while the other reactions are potentially instantaneous under the investigated conditions.

demonstrating only a weak reversible interaction of carbon in methane with the catalyst. Moreover, the fact that the $^{12}CH_4$ transient trails the inert response while the $^{12}C_2H_4$ does not differ significantly from it indicates that there are two possible reaction routes available for methane; there is one route in which methane reacts to, in general, C_{2+} products without any significant interaction with the catalyst and another in which methane shows a small reversible interaction with the catalyst, but which does not lead to C_{2+} products. The former reaction route could be assigned to a reversible heterolytic activation of methane, while the latter route could correspond to the homolytic production of methyl radicals. At first sight, ethene is expected to exhibit a stronger interaction with the catalyst than methane because of the double bond in ethene. The high basicity of Sn/Li/MgO probably prevents the interaction of ethene with the catalyst. It is clear that the latter improves the selectivity of the catalyst.

The $^{12}CO_2$ transient is slow as compared to the inert response, indicating a strong interaction with the catalyst of carbon atoms leading to carbon dioxide.

REACTION MECHANISM

A reaction mechanism, shown in Table 2, was developed with which it was possible to describe the experiments adequately with physically realistic and statistically significant kinetic parameter estimates. Only the reactions concerning experimentally observed products and reactants are considered. The production of propane is not taken into account because of the small selectivity towards propane. The reaction steps depicted in bold, reactions 1, 2, 4, 5, 7, 8, and 10, are assumed to be kinetically significant while the other reaction steps, reactions 3, 6, and 9, are assumed to be potentially instantaneous. The kinetically significant reactions are all assumed to be elementary, in the sense that their reaction rates can be calculated using the law of mass action. With these assumptions the kinetically significant gas-phase components are oxygen, methane, water, ethane, ethene, carbon dioxide, and methyl radicals. The kinetically significant species on the catalyst are oxygen atoms and methoxy species, CH_3O*. Further, lattice oxygen in the bulk of the oxide catalyst needs to be considered. Because of the high dilution of the gas flow, reaction 4 is assumed to be the only kinetically significant gas-phase reaction. This assumption is justified by the fact that even for undiluted gas streams, the contributions of gas-phase reactions other than the recombination of methyl radicals, i.e., reaction 4, are small as compared to the catalytic reactions, as was shown by Couwenberg (19) for the lined-out Li/Sn/MgO catalyst.

Activation of Oxygen

For all catalysts, except for lined-out Li/MgO, the experiments indicate a strong interaction of oxygen with the catalyst, reversible dissociative adsorption of oxygen, and exchange of oxygen on the catalyst with lattice oxygen in the bulk of the oxide catalyst. The lattice oxygen in the solid becomes available for exchange by diffusion of oxygen in the oxide structure, which is generally believed to take place via a vacancy mechanism (27–29). No significant exchange was observed with lined-out Li/MgO, probably because of the loss of lithium during the line-out, see Table 1. Hence, it seems probable that on the lithium-promoted catalysts the oxygen involved in the isotope exchange is present as a lithium oxide phase. The latter agrees with the large interaction of oxygen with lined-out Sn/Li/MgO, which still contains a large amount of lithium after the line-out procedure. The decrease of the interaction of oxygen with Li/MgO during the line-out procedure could be connected to the observed decrease of activity of the Li/MgO catalyst for the oxidative coupling of methane during the line-out procedure. The high specific surface area of pure MgO, as compared to that of the lithium-promoted catalysts, probably provides the exchangeable oxygen necessary for a large interaction of oxygen with MgO. The effects of the promotion with lithium and tin will be determined more exactly from the results of modelling the transient isotope responses over the various catalysts as described below. Also described below are the results of modelling the oxygen isotope experiments in the absence of reaction. Reaction 1 was selected for describing the

reversible dissociative adsorption of oxygen after discrimination between several rival models. Other plausible reaction mechanisms, such as molecular adsorption of oxygen followed by dissociation in a second step, were rejected because of physically unrealistic values for the kinetic parameters or because the regression results were worse than those corresponding to reaction 1. Reaction 1 closely resembles the oxygen activation proposed by Ito *et al.* (30). The free sites in reaction 1, denoted by an asterisk, can be compared to the oxygen vacancies at the catalyst surface in the description of Ito *et al.*

Reaction 10 describes the exchange between oxygen on the catalyst and lattice oxygen in the bulk of the catalyst.

Activation of Methane

The methane responses were not regressed because of their rapid relaxations as compared to the inert response. Therefore the small reversible interaction of methane with the catalyst is not taken into account in the reaction mechanism presented in Table 2. Reaction 2 describes the production of methyl radicals as an Eley–Rideal reaction between oxygen on the catalyst and methane from the gas phase. Reaction 3 describes the regeneration of adsorbed oxygen, O^*. Reactions 1, 2, and 3 are similar to the reactions proposed by Ito *et al.* (30) for the production of methyl radicals from oxygen and methane in the presence of lithium-promoted magnesia. The assumption that under the investigated conditions the C–H bond breaking in reaction 2 is rate controlling rather than the regeneration of active sites in reaction 3, is in agreement with studies in which deuterium-labelled methane was used to examine kinetic isotope effects (31, 32).

Production of C_2 Products

The experiments with deuterium-labelled ethane also provide strong indications for the direct homogeneous coupling of methyl radicals, presented by reaction 4 (31). The coupling of methyl radicals in the gas phase was confirmed by experiments using temporal analysis of products (TAP). At pressures sufficiently low to inhibit gas-phase reactions methyl radicals but no ethane were detected (33, 34). Reactions 5 and 6 describe the dehydrogenation of ethane to ethene by oxygen on the catalyst. The production of ethene as described above is in agreement with the methane isotope step experiment under coupling reactions, Fig. 6; no carbon-containing intermediates interacting significantly with the catalyst are involved in the reaction path to ethene.

Production of Carbon Dioxide

In the absence of reaction a large interaction of carbon dioxide with fresh Li/MgO and Sn/Li/MgO and a weak interaction with MgO and lined-out Li/MgO was observed. The large decline of the interaction of carbon dioxide with the Li/MgO catalyst because of the line-out procedure is probably caused by the loss of lithium. Apparently, lithium is necessary for a large interaction of carbon dioxide with the catalyst. This result is not surprising, since carbon dioxide can convert lithium oxide, Li_2O, into lithium carbonate, Li_2CO_3. This carbonate phase is believed to be the pool for the exchange of carbon in carbon dioxide in case of both fresh Li/MgO and Sn/Li/MgO in the absence of reaction. Under reaction conditions a strong interaction with lined-out Sn/Li/MgO of both the oxygen and carbon atoms leading to carbon dioxide was observed. This could be caused by the formation of carbon dioxide on the catalyst and/or interaction of carbon dioxide from the gas phase with the catalyst. In the reaction mechanism in Table 2 interaction of carbon dioxide from the gas phase with the catalyst is not included, because modelling of the experiments over lined-out Sn/Li/MgO under reaction conditions showed that this interaction can be neglected compared with the interaction due to the surface-catalyzed formation of carbon dioxide from methane and oxygen via reactions 7 to 9. Although not measured, it seems probable that the interaction of carbon dioxide from the gas phase with lined-out Sn/Li/MgO is at least weaker than with fresh Sn/Li/MgO, because the catalyst loses lithium during the line-out procedure, as can be seen in Table 1. Moreover, under reaction conditions oxygen and water may be present on the catalyst, preventing a large interaction of carbon dioxide from the gas phase with the catalyst. Reaction 7 describes the formation of a methoxy species on the catalyst. Both methane and methyl radicals are assumed to react with the same type of adsorbed oxygen atoms, O^*, which is probably a simplification of the actual mechanism. In reactions 8 and 9 this methoxy species is transformed to carbon dioxide. Reaction 9 is assumed to be potentially instantaneous and is shown only for stoichiometric reasons. A single kinetically significant carbon-containing species on the catalyst in the reaction path to carbon dioxide is considered because the slope of the $^{12}CO_2$ response of the methane isotope step experiment under coupling conditions (see Fig. 6) is different from zero at $t = 0$ (4, 11). In the case that more than one carbon-containing intermediate interacts significantly with the catalyst, the slope of the $^{12}CO_2$ transient should be zero at time $t = 0$. The choice for a methoxy species as the intermediate in the reaction path to carbon dioxide was based on the results of simultaneous modelling of the methane and oxygen isotope step experiments under coupling conditions, among other results. It was not possible to obtain acceptable simulations if the carbon/oxygen ratio in the carbon-containing intermediate on the catalyst in the reaction path to carbon dioxide was not equal to one, such as in CO_2^* or CO_3^*. Many authors mention a methoxy species as an intermediate in the reaction path to carbon dioxide (30, 35–39). Moreover, the existence of methoxy species on the catalyst was shown

experimentally under conditions typical for the oxidative coupling of methane (40–42). The primary production of carbon dioxide, as described above, is in agreement with the experiments carried out by Couwenberg *et al.* (19), who found that for the lined-out Li/Sn/MgO catalyst, the selectivity towards C_{2+} products was only a weak function of the space time. If the oxidation of C_{2+} products were to have a large contribution to the production of CO_x, the selectivity should decrease at increasing space time. Nelson and Cant (43) found that below 1013 K the secondary production of CO_x from C_2 products on a Li/MgO catalyst was only a minor source of CO_x production. Because of the high basicity of Li/Sn/MgO as compared to Li/MgO, it seems reasonable to neglect the production of CO_2 from C_2 products for the Li/Sn/MgO catalyst at the temperature 1023 K used in this work.

REGRESSION RESULTS

To further validate the adequacy of the reaction mechanism shown in Table 2, it was used to describe quantitatively the oxygen isotope step experiments in the absence of reaction as well as the oxygen and methane isotope step experiments under reaction conditions. According to Table 2, the expressions for the net production rates of the ^{18}O-labelled gas-phase and surface components, to be substituted in Eqs. [2] and [3], are as follows:

gas phase:

$$R_{18_{O_2}} = \frac{k_{-1}}{L_t} L_{18_O}^2 - \frac{k_1}{L_t} C_{18_{O_2}} L_*^2 \quad [8]$$

$$R_{16_O 18_O} = 2\frac{k_{-1}}{L_t} L_{18_O}(L_O - L_{18_O}) - \frac{k_1}{L_t} C_{18_O 16_O} L_*^2 \quad [9]$$

$$R_{C^{18}O_2} = \frac{k_8}{L_t} L_{CH_3^{18}O} L_{18_O} \quad [10]$$

$$R_{C^{16}O^{18}} = \frac{k_8}{L_t} L_{CH_3^{18}O} L_O - L_{18_O}) + \frac{k_8}{L_t}(L_{CH_3O} - L_{CH_3^{18}O}) L_{18_O} \quad [11]$$

surface:

$$R_{18_{O^*}} = 2\frac{k_1}{L_t} C_{18_{O_2}} L_*^2 + \frac{k_1}{L_t} C_{16_O 18_O} L_*^2 - 2\frac{k_{-1}}{L_t} L_{18_O}^2 - 2\frac{k_{-1}}{L_t} L_{18_O}(L_O - L_{18_O}) - \frac{1}{2} k_2 C_{CH_4} L_{18_O} - k_5 C_{C_2H_6} L_{18_O} - k_7 C_{CH_3\cdot} L_{18_O} - \frac{5}{2}\frac{k_8}{L_t} L_{CH_3O} L_{18_O} - \alpha_s \varphi_{18_O}(x,t) \quad [12]$$

$$R_{CH_3^{18}O_*} = k_7 C_{CH_3\cdot} L_{18_O} - \frac{k_8}{L_t} L_{CH_3^{18}O} L_O. \quad [13]$$

An expression for φ_{18_O} (mol m_{CAT}^{-2} s^{-1}), the flux of ^{18}O atoms towards the bulk of the catalyst, is derived in Appendix B.

The expressions for the net production rates of the ^{13}C-labelled gas phase and surface components, to be substituted in Eqs. [2] and [3], are as follows:

gas phase:

$$R_{13_{CH_4}} = -k_2 C_{13_{CH_4}} L_O \quad [14]$$

$$R_{13_{CO_2}} = \frac{k_8}{L_t} L_{13_{CH_3O}} L_O \quad [15]$$

surface:

$$R_{13_{CH_3O\cdot}} = k_7 L_O C_{CH_3\cdot} \frac{C_{13_{CH_4}}}{C_{CH_4}} - \frac{k_8}{L_t} L_{13_{CH_3O}} L_O. \quad [16]$$

L_* denotes the concentration of free sites available for oxygen adsorption on the catalyst (mol kg_{CAT}^{-1}). The exact nature of these sites is not clear but they could be oxygen vacancies at the catalyst surface. L_* is calculated from $L_* = L_t - L_O - L_{CH_3O}$, where L_t is the total concentration of sites on the catalyst available for exchange (mol kg_{CAT}^{-1}). L_O is the concentration of oxygen on the catalyst (mol kg_{CAT}^{-1}), available for exchange with gas-phase oxygen or lattice oxygen in the oxide structure as well as for reaction with methane, ethane, methyl radicals, and methoxy species. The oxygen corresponding to L_O can be oxygen atoms simply adsorbed on the catalyst or present in the form of an oxide phase. Bulk lattice oxygen is not directly available for exchange or reaction and is therefore not included in the value of L_O. Boreskov (26), Klier *et al.* (24), and Winter (25) described oxygen exchange between gas-phase oxygen and solid oxides with three global reactions in which either one, two, or no oxygen atoms of an oxygen molecule are exchanged with the solid. Using this approach, the detailed reaction mechanism is not important. Moreover, diffusion of oxygen in the solid was either neglected or assumed to be infinitely fast. In this work, the reactions which are directly responsible for the exchange between gas-phase oxygen and the solid oxide are considered explicitly and, hence, values for the corresponding kinetic parameters, i.e., the oxygen adsorption and desorption rate coefficients and the diffusion coefficients of oxygen in the oxide structure, can be obtained. The reaction rates of the elementary steps are calculated according to the law of mass action, neglecting kinetic isotope effects and assuming that all exchangeable species

TABLE 3

Estimates for the Rate of Adsorption and Desorption, the Concentration of Oxygen on the Catalyst and the Diffusion Coefficient of Oxygen in the Bulk of the Catalyst with Their 95% Confidence Intervals Obtained by Regression of the Oxygen Isotope Step Experiments in the Absence of Reaction at T = 1023 K

Catalyst	C_{O_2} (mol m_{gas}^{-3})	r_w (mol kg_{CAT}^{-1} s^{-1})	L_O (mol kg_{CAT}^{-1} (mol m_{CAT}^{-2}))[a]	D_0 (m_{CAT}^3 m_{CAT}^{-1} s^{-1})
MgO	0.19	$5.2 \pm 0.3 \times 10^{-3}$	$8 \pm 2 \times 10^{-2}$ ($2.6 \pm 0.6 \times 10^{-6}$)	$2.10 \pm 0.01 \times 10^{-22}$
Fresh Li/MgO	0.24	$5.6 \pm 0.1 \times 10^{-3}$	$1.98 \pm 0.06 \times 10^{-2}$ ($3.3 \pm 0.1 \times 10^{-5}$)	$4.04 \pm 0.01 \times 10^{-20}$
Fresh Sn/Li/MgO	0.24	$1.4 \pm 0.1 \times 10^{-2}$	$2.7 \pm 0.1 \times 10^{-1}$ ($1.34 \pm 0.06 \times 10^{-4}$)	$1.51 \pm 0.01 \times 10^{-19}$

[a] L_O in the units mol m_{CAT}^{-2} is equal to L_O in the units mol kg_{CAT}^{-1} divided by α_s.

on the catalyst are equivalent and distributed at random. Hence, the rates of the elementary steps are equal to the product of a reaction rate coefficient and the concentrations of the corresponding (labelled) species. The factor 2 in Eqs. [9] and [12] is caused by the equivalence of $^{16}O^{18}O$ and $^{18}O^{16}O$. Although methyl radicals are kinetically significant intermediates according to the reaction mechanism presented in Table 2, it is not necessary to formulate to formulate the continuity equation for $^{13}CH_3\cdot$ if methyl radicals are assumed to react very fast as compared to their production. In that case the steady-state approximation is valid for methyl radicals and the concentration of labelled methyl radicals can be calculated from the concentration of labelled methane via the following relation: $C_{^{13}CH_3\cdot}/C_{CH_3\cdot} = C_{^{13}CH_4}/C_{CH_4}$.

Oxygen Isotope Steps in the Absence of Reaction

In the absence of reaction the oxygen isotope responses are simulated by integration of Eqs. [2] and [3], with the corresponding net production rates [8], [9], and [12]. The rate of oxygen adsorption, $r_1 = \frac{k_1}{L_t} C_{O_2} L_*^2$, is equal to the rate of oxygen desorption, $r_{-1} = \frac{k_{-1}}{L_t} L_O^2$. Thus $r_1 = r_{-1} = r_w$ (mol kg_{CAT}^{-1} s^{-1}). Introducing this expression in Eqs. [8], [9], and [12] reduces the number of parameters to three, i.e., r_w, L_O, and D_O. For MgO and fresh Li/MgO and Sn/Li/MgO the estimated values for these parameters with their 95% confidence intervals are presented in Table 3. The concentration of oxygen on the catalyst, L_O, is also given in the units mol m_{CAT}^{-2} to facilitate the comparison of the catalysts. As an example the calculated oxygen isotope responses corresponding to the experiment over fresh Sn/Li/MgO is the absence of reaction are given in Fig. 1. The effects of promotion with lithium and tin can be determined from the comparison of the three catalysts. The estimates for r_w are approximately equal for MgO and Li/MgO while the value of r_w for Sn/Li/MgO is significantly higher. The concentration of oxygen on the catalyst in the units mol m_{CAT}^{-2} increases considerably from MgO to Sn/Li/MgO. For MgO the concentration of oxygen on the catalyst amounts to only 10% of a theoretical monolayer, which is 2×10^{-5} mol m_{CAT}^{-2}, while for the lithium-promoted catalysts, especially for Sn/Li/MgO, the value of a theoretical monolayer is exceeded. Peil *et al.* (8) attributed this phenomenon to subsurface oxygen immediately available for oxygen exchange. Alternatively, on MgO oxygen is simply adsorbed, while on the lithium-promoted catalysts oxygen is present in the form of a lithium oxide phase. In both hypotheses, especially for the lithium-promoted catalysts, the units mol kg_{CAT}^{-1} are more appropriate than the units mol m_{CAT}^{-2}. The high specific surface area is responsible for a large amount of exchangeable oxygen on MgO, as can be seen from the value of L_O in mol kg_{CAT}^{-1} as compared to the value in mol m_{CAT}^{-2}. The only value for the diffusion coefficient of lattice oxygen in MgO at 1023 K found in are literature amounts to 10^{-24} m_{CAT}^3 m_{CAT}^{-1} s^{-1} (27). Considering the large differences in reported values at other temperatures the estimated value of D_O presented in Table 3 is of the proper order of magnitude. Peil *et al.* (8) estimated D_O for MgO and Li/MgO from the offset of the $^{16}O^{18}O$ signal and found similar values. The promotion with both lithium and tin increases the mobility of lattice oxygen in the bulk of the catalyst, as can be seen from the increased value of D_O for the lithium-promoted catalysts and even more for the tin/lithium-promoted catalysts as compared to the unpromoted MgO catalyst. This could be the result of an increase in the number of oxygen vacancies in the MgO crystal. Lacy *et al.* (28) proposed the following mechanism for the formation of oxygen vacancies in the MgO lattice due to the promotion with lithium. For every two Li^+ ions leaving the Li_2O precipitate only one Mg^{2+} leaves the MgO crystal. From stoichiometric considerations the lack of oxygen atoms, or the excess of cations, in the crystal can result in the formation of oxygen vacancies. The increase of D_O due to promotion with lithium and tin explains inter alia the observed increase of activity of the MgO catalyst for the oxidative coupling of methane after promotion with lithium and tin (18), possibly because

TABLE 4

Estimates with Their 95% Confidence Intervals for the Kinetic Parameters Obtained by the Simultaneous Regression of the Oxygen and Methane Isotope Step Experiments in the Presence of Reaction over Lined-Out Sn/Li/MgO[a]

Parameter	Value
$k_1 L_t$ (m^3_{gas} kg^{-1}_{CAT} s^{-1})	$3.5 \pm 0.1 \times 10^{-2}$
$k_{-1} L_t^{-1}$ (kg_{CAT} mol^{-1} s^{-1})	$1.3 \pm 0.1 \times 10^{-3}$
k_2 (m^3_{gas} mol^{-1} s^{-1})	$1.75 \pm 0.05 \times 10^{-3}$
k_7 (m^3_{gas} mol^{-1} s^{-1})	5.1 ± 0.6
$k_8 L_t^{-1}$ (kg_{CAT} mol^{-1} s^{-1})	$2.73 \pm 0.07 \times 10^{-3}$
D_O (m^3_{CAT} m^{-1}_{CAT} s^{-1})	$5 \pm 1 \times 10^{-20}$

[a] Reaction conditions: T = 1023 K, initial molar ratio CH_4/O_2 = 4, 80% helium dilution, X_{CH_4} = 24%, X_{O_2} = 85%, $S_{C_2H_6}$ = 31%, $S_{C_2H_4}$ = 23%, $S_{C_3H_8}$ = 2%, and S_{CO_2} = 44%.

of an increased oxygen activation due to an increased number of oxygen vacancies at the catalyst surface.

Isotope Steps in the Presence of Reaction

The $^{18}O_2$, $^{18}O^{16}O$, $C^{18}O_2$, $C^{18}O^{16}O$, and $^{13}CO_2$ responses in the presence of reaction were regressed simultaneously to obtain a single set of statistically significant and physically realistic estimates for the kinetic parameters. It was necessary to take the steady-state axial total concentration profiles, calculated according to Eq. [5] and [6], into account as they had a significant influence on the transient isotope responses. Because the inlet methane to oxygen ratio was much higher than the stoichiometric one, the methane concentration could, however, be assumed constant through the bed and equal to the mean of the inlet and outlet concentrations. The estimates of the kinetic parameters with their 95% confidence intervals are presented in Table 4. The largest value of the binary correlation coefficient between the parameter estimates was 0.91.

As can be seen from Table 4, the parameter L_t was not estimated individually but had to be lumped with, respectively, the parameters k_1, k_1, and k_8 to obtain statistically significant estimates. This was necessary because under the investigated conditions L_* was approximately equal to L_t. The value of k_4 does not influence the shape of the transient isotope responses. Therefore k_4 was not estimated by regression but calculated using expressions from the literature, taking into account the temperature-dependent pressure fall-off behaviour of k_4 (2, 19). At atmospheric pressure and 1023 K the value of k_4 is equal to 1.21×10^4 m^6_{gas} mol^{-1} kg^{-1}_{CAT} s^{-1}. The value of k_5 was calculated from the value of k_2 using collision theory to relate the preexponential factors (44) and the Polanyi–Semenov equation (44, 45) to relate the activation energies. In this study the difference in the activation energies of k_2 and k_5 was taken as equal to the difference in the standard reaction enthalpies of reactions 2 and 5, i.e., 20 kJ mol^{-1} (46). According to these assumptions, the relation between k_5 and k_2 at 1023 K is $k_5 = 7.67\ k_2$. All estimates presented in Table 4 are within the range of physically realistic values (47, 48) expected for rate coefficients corresponding to the elementary steps shown in Table 2.

The calculated responses of $^{18}O_2$, $^{16}O^{18}O$, $C^{18}O_2$, and $C^{16}O^{18}O$, corresponding to the oxygen isotope step experiment and the calculated $^{12}CO_2$ response, obtained from the $^{13}CO_2$ response, corresponding to the methane isotope step experiment, are shown in Figs. 3, 4, and 6. The initial rapid relaxation of the oxygen responses is only partially simulated, especially the initial rapid relaxation of the $^{16}O^{18}O$ signal. Note that the calculated ratio $\frac{C^2_{^{16}O^{18}O}}{C_{^{18}O_2} C_{^{16}O_2}}$ in the presence of reaction is adequately simulated, viz. Fig. 5. The calculated steady-state axial total concentration profiles of O_2, CO_2, C_2H_6, C_2H_4, and $CH_3\cdot$ are shown in Fig. 7 and the corresponding profiles of O* and CH_3O* are shown in Fig. 8. With the set of kinetic parameters given in Table 4, not only reasonable agreement between the experimental and calculated transient isotope responses of both the oxygen and methane isotope step experiments was obtained. The steady-state outlet concentrations of oxygen, carbon dioxide, ethane, and ethene were also calculated adequately, as can be seen in Fig. 7.

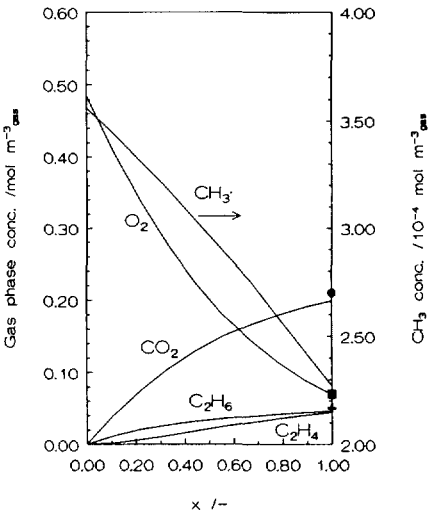

FIG. 7. Steady-state axial total concentration profiles of oxygen, carbon dioxide, ethane, ethene, and methyl radicals in the gas phase, calculated with the set of parameters given in Table 4 by integration of Eq. [5] and simultaneously solving Eq. [6]. The $CH_3\cdot$ concentration is calculated assuming the pseudo-steady state for methyl radicals. The methane concentration has a constant value of 1.7 mol m^3_{gas}. Observed outlet concentrations: ●, CO_2; □, O_2; ◆, C_2H_6; +, C_2H_4.

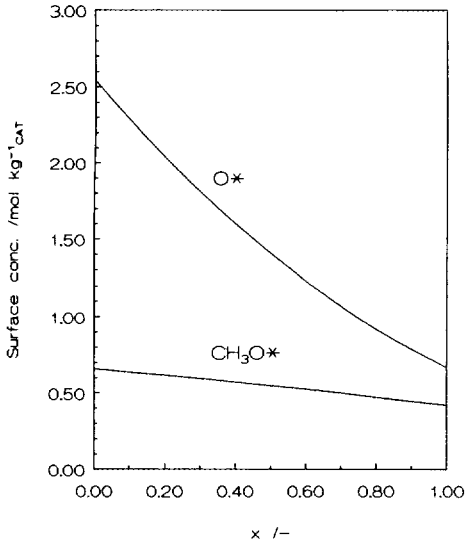

FIG. 8. Steady-state axial total concentration profiles of oxygen atoms and methoxy species on the catalyst, calculated with the set of parameters given in Table 4 by integration of Eq. [5] and simultaneously solving Eq. [6].

If the oxygen isotope responses are simulated with the values of $k_1 L_t$, $k_{-1} L_t^{-1}$, and D_O from Table 4 and with the values of the other parameters equal to zero, i.e., in the absence of reaction, the oxygen isotope responses are indeed similar to those obtained in the absence of reaction (Fig. 1). In the absence of reaction the estimated value of L_O on lined-out Sn/Li/MgO was 2.00 ± 0.05 mol kg_{CAT}^{-1}, which is comparable to L_O in the presence of reaction (Fig. 8). Thus the differences between the oxygen isotope responses in the absence and in the presence of reaction are not caused by a decrease in exchange sites for oxygen. Apparently the reactions on the catalyst cause the initial rapid relaxation of the oxygen signals. The value of L_O on lined-out Sn/Li/MgO is larger than the value estimated for fresh Sn/Li/MgO (see Table 3), possibly because the concentration of gas-phase oxygen in the experiment with lined-out Sn/Li/MgO was higher by a factor of two as compared with the experiment with the fresh catalyst, or because the line-out procedure alters the oxygen adsorption and/or desorption rate coefficients.

The estimated value of the diffusion coefficient of lattice oxygen, D_O, from Table 4 is lower than the value of D_O estimated for the oxygen isotope experiment in the absence of reaction over lined-out Sn/Li/MgO, which was 3.36 ± 0.09 × 10^{-19} m_{CAT}^3 m_{CAT}^{-1} s^{-1} (not shown in the tables). The difference could be caused by the presence of a carbonate phase on the catalyst under reaction conditions, which could result in a decrease in the amount of lithium in the MgO lattice or a decrease in the number of oxygen vacancies as compared with the situation in which no carbonate phase is present on the catalyst. The concentrations of both O* and CH_3O*, shown in Fig. 8, are too large to be explained by simple adsorption. Probably both species are present as or in an extra phase, such as lithium oxide or lithium carbonate, as was already suggested for the existence of oxygen on the lithium-promoted catalysts in the absence of reaction. In this context it should be mentioned that the methoxy species must in fact be seen as a CH_xO* species. The number of hydrogen atoms in this species cannot be determined because only oxygen and carbon isotope step experiments were carried out.

Further extensions of the presented model can be proposed, for example the use of a heterogeneous instead of a homogeneous model, i.e., to make a distinction between the catalyst pellets and the fluid phase. It is expected, however, that these extensions will have only a marginal influence on the results presented in this work.

In this study, the experiments under coupling conditions were carried out only over lined-out Sn/Li/MgO. In the absence of reaction, the effects of promotion with lithium and tin were determined from the experiments with the corresponding catalysts. A similar approach under reaction conditions would give information about the effects of promotion on each of the kinetic parameters given in Table 4.

CONCLUSIONS

Both in the absence and presence of reaction, oxygen interacts strongly with the catalysts. The exception is provided by lined-out Li/MgO, probably because of the loss of lithium during the line-out procedure. Oxygen displays reversible dissociative adsorption and exchange between oxygen on the catalyst and lattice oxygen in the bulk of the catalyst. The promotion with lithium, and even more with tin, increases the diffusion coefficient of oxygen in the bulk of the catalyst and the amount of exchangeable oxygen on the catalyst per unit BET surface area. Two possible reaction routes are available for methane; there is one route in which methane reacts to C_2 products without any significant interaction with the catalyst and another in which methane shows a weak reversible interaction with the catalyst, but which does not lead to C_2 products. In the absence of reaction, a strong interaction of carbon dioxide with the catalyst is only possible if lithium is present in large amounts. The experiments under reaction conditions can be described satisfactorily with a methoxy species on the catalyst as intermediate in the reaction route to carbon dioxide.

The above conclusions could only be reached using quantitative descriptions of the isotopic transients. Validation of and discrimination between reaction mechanisms was possible on the basis of their ability to quantitatively describe the isotopic transients. Moreover, values for reac-

tion rate coefficients, surface concentrations, and, in this study, the diffusion coefficient of oxygen in the oxide catalyst could be obtained from nonlinear multiresponse regression analysis. The most reliable model is developed if different kinds of isotope step experiments are regressed simultaneously, i.e., described with a single set of kinetic parameters. In an integral reactor it is necessary to take the steady-state axial total concentration profiles into account, because of the significant influence of the latter on the simulation of the transient isotope responses.

APPENDIX A: NOMENCLATURE

$\mathbf{b}$	parameter vector
C_i	concentration of gas-phase component i, mol m_{gas}^{-3}
D_O	diffusion coefficient of oxygen in the bulk of the catalyst, $m_{CAT}^3\ m_{CAT}^{-1}\ s^{-1}$
F_{TOT}	total molar flow rate, mol s^{-1}
f	function describing the inert response after switching between two gas mixtures
f_q	response calculated with the reactor model for response q
k_i	rate coefficient of reaction step i, units situation dependent
L_j	concentration of component j on the catalyst available for exchange, mol kg_{CAT}^{-1}
L_t	total concentration of sites on the catalyst available for exchange, mol kg_{CAT}^{-1}
L_*	concentration of free sites on the catalyst available for oxygen adsorption, mol kg_{CAT}^{-1}
N_O	oxygen concentration in the bulk of the catalyst, mol m_{CAT}^{-3}
n	number of experiments
R_i	net production rate of component i, mol $kg_{CAT}^{-1}\ s^{-1}$
r	position in a catalyst particle, defined as the distance from the surface, m
r_i	reaction rate of reaction step i, mol $kg_{CAT}^{-1}\ s^{-1}$
r_W	rate of oxygen adsorption and desorption in the absence of reaction, mol $kg_{CAT}^{-1}\ s^{-1}$
S	objective function
S_i	selectivity towards product i with respect to methane, %
T	temperature, K
t	time, s
V_{mol}	molar volume, $m_{gas}^3\ mol^{-1}$
v	number of responses
W_{CAT}	total catalyst mass, kg_{CAT}
X_i	conversion of reactant i, %
x	dimensionless axial reactor position
$\mathbf{x}_i$	vector of set variables for experiment i
y_i	fraction of component i in the gas phase
$y_{i,q}$	qth experimental response in the ith experiment

Greek Symbols

α_s	specific surface area of the catalyst, $m_{CAT}^2\ kg_{CAT}^{-1}$
ε_B	bed porosity, $m_{gas}^3\ m_{bed}^{-3}$
ξ_{18_O}	isotope fraction ^{18}O in the bulk of the catalyst
ρ_B	bed density, $kg_{CAT}\ m_{bed}^{-3}$
σ^{qr}	element (q, r) of the inverse error covariance matrix
τ	residence time in the reactor, s
φ_O	oxygen flux to and from the bulk of the catalyst, mol $m_{CAT}^{-2}\ s^{-1}$
X_{18_O}	isotope fraction ^{18}O on the catalyst

Superscripts

$'$	labelled
0	reactor inlet

APPENDIX B: EXPRESSION FOR THE FLUX OF ^{18}O ATOMS INTO THE BULK OF THE CATALYST

In the oxygen isotope step experiments exchange between oxygen atoms on the catalyst and lattice oxygen in the bulk of the oxide catalyst was observed. The flux of ^{18}O atoms towards the bulk of the catalyst is calculated from the continuity equation for ^{18}O in the bulk lattice of the catalyst, which, assuming a slab geometry, corresponds to Fick's second law for ^{18}O in the solid phase,

$$\frac{\partial \xi_{18_O}}{\partial t} = D_O \frac{\partial^2 \xi_{18_O}}{\partial r^2} \qquad [1]$$

Initial condition:

$$t = 0 \quad \forall r \qquad \xi_{18_O} = 0 \qquad [2a]$$

Boundary conditions:

$$t > 0 \quad r = 0 \qquad \xi_{18_O} = X_{18_O} \qquad [2b]$$

$$t > 0 \quad r = \infty \qquad \xi_{18_O} = 0 \qquad \text{(semi-infinite solid)}, \qquad [2c]$$

where ξ_{18O} is the isotope fraction ^{18}O in the bulk lattice of the catalyst (−), X_{18_O} is the isotope fraction ^{18}O on the catalyst, D_O is the diffusion coefficient of lattice oxygen in the bulk of the catalyst ($m_{CAT}^3\ m_{CAT}^{-1}\ s^{-1}$), and r the position in a catalyst particle, defined as the distance to the surface [m].

The flux φ_{18_O} at the surface of the catalyst is calculated via Fick's first law,

$$\varphi_{18_O} = -N_O D_O \left.\frac{\partial \xi_{18_O}}{\partial r}\right|_{r=0}, \qquad [3]$$

where N_O is the oxygen concentration in the bulk [mol m_{CAT}^3], calculated by dividing the catalyst density by its molecular weight.

Integration of Eq. [1] and substitution of the result in Eq. [3] leads to the following expression for φ_{18_O}:

$$\varphi_{18_O} = \sqrt{D_O}\, N_O \frac{1}{\sqrt{\pi}} \int_0^t \frac{1}{\sqrt{t-\tau}} \frac{\partial X_{18_O}}{\partial t}\bigg|_\tau d\tau. \qquad [4]$$

This integral can be quadratured as

$$\varphi_{18_O,n} = 2\sqrt{D_O}\, N_0 \frac{1}{\sqrt{\pi}} \qquad [5]$$
$$\left[\sum_{k=0}^{n-1} \frac{X_{18_O,k+1}(X) - X_{18_O,k}(X)}{t_{k+1} - t_k} \{\sqrt{t_n - t_k} - \sqrt{t_n - t_{k+1}}\}\right],$$

where $\varphi_{18_O,n}$ is the flux at time t_n and position x in the reactor.

ACKNOWLEDGMENT

This work was funded in part by the Commission of the European Communities in the framework of the Joule programme, subprogramme Energy from Fossil Sources, Hydrocarbons, No. JOUF-0044-C.

REFERENCES

1. Chen, Q., Hoebink, J. H. B. J., and Marin, G. B., *Ind. Eng. Chem. Res.* **30,** 2088 (1991).
2. Chen, Q., Couwenberg, P. M., and Marin, G. B., *AlChE J.* **40,** 521 (1994).
3. Zanthoff, H., and Baerns, M., *Ind. Eng. Chem. Res.* **29,** 2 (1990).
4. Happel, J., "Isotopic Assessment of Heterogeneous Catalysis." Academic Press, New York, 1986.
5. Biloen, P., Helle, J. N., van den Berg, F. G. A., and Sachtler, W. H. M., *J. Catal.* **81,** 450 (1983).
6. Happel, J., Suziki, I., Kokayeff, P., and Fthenakis, V., *J. Catal.* **65,** 59 (1980).
7. Sun, Y.-K., Lewandowski, J. T., Myers, G. R., Jacobson, and A. J., Hall, R. B., *in* "The Activation of Dioxygen and Homogeneous Catalytic Oxidation" (H. R. Barton, A. E. Martel and D. Sawyer, Eds.), p. 97. Plenum, New York, 1993.
8. Peil, K. P., Goodwin, J. G., and Marcelin, G., *J. Catal.* **131,** 143 (1991).
9. Peil, K. P., Goodwin, J. G., and Marcelin, G., *J. Phys. Chem.* **93,** 5977 (1989).
10. Peil, K. P., Goodwin, J. G., and Marcelin, G., *J. Am. Chem. Soc.* **112,** 6129 (1990).
11. Mirodatos, C., *Catal. Today* **9,** 83 (1991).
12. Mirodatos, C., Holmen, A., Mariscal, R., and Martin, G. A., *Catal. Today* **6,** 601 (1990).
13. Miro, E., Santamaria, J., and Wolf, E. E., *J. Catal.* **124,** 451 (1990).
14. Lacombe, S., Sanchez M., J. G., Delichere, P., Mozzanega, H., Tatibouet, J. M., and Mirodatos, C., *Catal. Today* **13,** 273 (1992).
15. Driscoll, S. A., and Okzan, U. S., *J. Phys. Chem* **97,** 11524 (1993).
16. Driscoll, S. A., Gardner, D. K., and Ozkan, U. S., *Catal. Lett.* **25,** 191 (1994).
17. Happel, J., Walter, E., and Lecourtier, Y., *J. Catal.* **123,** 12 (1990).
18. Korf, S. J., Roos, J. A., van Ommen, J. G., and Ross, J. R. H., *Appl. Catal.* **56,** 119 (1989).
19. Couwenberg, P. M., Ph.D. dissertation, Eindhoven University of Technology, 1995.
20. Verwer, J. G., Blom, J. G., Furzeland, R. M., and Zegeling, P. A., *in* "Adaptive Methods for Partial Differential Equations" (J. E. Flaherty, P. J. Paslow, M. S. Shephard and J. D. Vasilakis, Eds.), p. 160. SIAM, Philadelphia, 1989.
21. Numerical Algorithm Group "FORTRAN Library Manual, Mark 15," Oxford, 1991.
22. Marquardt, D. W., *J. Soc. Indust. Appl. Math.* **11,** 431 (1963).
23. Froment, G. F., and Hosten, L. H., *in* "Catalysis, Science and Technology" (J. R. Anderson and M. Boudart, Eds.), p. 98. Springer-Verlag, Berlin, 1981.
24. Klier, K., Nováková, J., and Jírů, P., *J. Catal.* **2,** 479 (1963).
25. Winter, E. R. S., *J. Chem. Soc. A,* 2889 (1968).
26. Boreskov, G. K., *Adv. Catal.* **15,** 285 (1964).
27. Yoo, H. I., Wuensch, B. J., and Petuskey, W. T., *in* "Advances in Ceramics" (W. D. Kingery, Ed.), Vol. 10, p. 394. American Ceramic Society, Ohio, 1983.
28. Lacy, J. B., Abraham, M. M., Boldú, J. L., Chen, Y., Narayan, J., and Tohver, H. T., *Phys. Rev. B* **18,** 4136 (1978).
29. Oishi, Y., and Ando, K., *in* "Advances in Ceramics" (W. D. Kingery, Ed.), Vol. 10, p. 379. American Ceramic Society, Ohio, 1983.
30. Ito, T., Wang, J., Lin, C., and Lunsford, J. H., *J. Am. Chem. Soc.* **107,** 5062 (1985).
31. Nelson, P. F., Lukey, C. A., and Cant, N. W., *J. Catal.* **120,** 216 (1989).
32. Cant, N. W., Lukey, C. A., Nelson, P. F., and Tyler, R. J., *J. Chem. Soc. Chem. Commun.* 767 (1988).
33. Buyevskaya, O. V., Rothaemel, M., Zanthoff, H., and Baerns, M., *J. Catal.* **146,** 346 (1994).
34. Mallens, E. P. J., Hoebink, J. H. B. J., and Marin, G. B., *Stud. Surf. Sci. Catal.* **81,** 205 (1994).
35. Tong, Y., and Lunsford, J. H., *J. Am. Chem. Soc.* **113,** 4741 (1991).
36. Iwamatsu, E., and Aika, K., *J. Catal.* **117,** 416 (1989).
37. McCarty, J. G., *in* "Methane Conversion by Oxidative Processes, Fundamental and Engineering Aspects" (E. E. Wolf, Ed.), p. 320. Van Nostrand–Reinhold, New York, 1992.
38. Aparicio, L. M., Rossini, S. A., Sanfilippo, D. G., Rekoske, J. E., Trevino, A. A., and Dumesic, J. A., *Ind. Eng. Chem. Res.* **30,** 2114 (1991).
39. Lehmann, L., and Baerns, M., *J. Catal.* **135,** 467 (1992).
40. Shafranovky, P. A., Sinev, M. Y., Zhizkin, G. N., and Shub, B. R., *Kinet. Katal.* **30,** 202 (1989).
41. Lo, M. Y., Agarwal, S. K., and Galya, L. G., *Catal. Today* **3,** 173 (1988).
42. Liu, H.-F., Liu, R.-S., Liew, K. Y., Johnson, R. E., and Lunsford, J. H., *J. Am. Chem. Soc.* **106,** 4117 (1984).
43. Nelson, P. F., and Cant N. W., *J. Phys. Chem.* **94,** 3756 (1990).
44. Boudart, M., and Djéga-Mariadassou, G., "Kinetics of Heterogeneous Catalytic Reactions." Princeton Univ. Press, Princeton, NJ, 1984.
45. Krylov, O. V., *Kinet. Katal.* **34,** 18 (1993).
46. Weast, R. C., "Handbook of Chemistry and Physics." CRC Press, Boca Raton, FL, 1987.
47. Zhdanov, V. P., Pavlíček, J., Knor, Z., *Catal. Rev. Sci. Eng.* **30,** 501 (1988).
48. Dumesic, J. A., Rudd, D. F., Aparicio, L. M., Rekoske, J. E., and Trevino, A. A., "The Microkinetics of Heterogeneous Catalysis." Am. Chem. Soc., Washington, DC, 1993.